

Topography from Topology: Photoinduced Surface Features Generated in Liquid Crystal Polymer Networks

Michael E. McConney, Angel Martinez, Vincent P. Tondiglia, Kyung Min Lee, Derrick Langley, Ivan I. Smalyukh, and Timothy J. White*

The ability of biological systems to self-assemble materials into pre-programmed shapes in response to external stimuli is inspirational. Emulating the capability of self-assembling, stimuli-responsive materials with tailored functionality (actuation, shape change, surface manipulation, or other property changes) is of paramount interest to fields ranging from biomedical engineering^[1] to robotics.^[2] Liquid crystalline phases and defects play a major role in the self-assembly of biological materials, including the plasma membrane, wood, silk, and the insect cuticle.^[3–6] Here, we examine the response of complexly patterned photoresponsive liquid crystal polymer networks (LCN). The rich and diverse topographical features reported here are retiscent to shape adaptations and topographical surface manipulation observable in nature and could be useful in a range of applications including haptic displays, optics/phonics, flow control, or even catalysis.

Liquid crystalline materials have repeatedly been demonstrated to exhibit a diverse range of stimuli-responsive behavior, such as negative thermal expansion and multi-stage phase transitions.^[7,8] The responsive nature of liquid crystal polymers are enabled and controlled by the anisotropic orientation of the mesogenic moieties. Azobenzene-functionalized LCN (azo-LCN) materials have been the subject of considerable recent examinations as adaptive materials^[9–18] and shape memory polymers.^[19–21] Importantly for the work presented here, the directionality of the strain generated with a stimulus in aligned LCN

materials (monodomain, twisted nematic, splay) is dictated by the director orientation of the material. For example, strain generated in a monodomain (nematic) LCN is primarily observed parallel to the alignment of the mesogens.^[16,22] Offsetting the orientation of the director profile to the sample geometry (film or cantilever) results in out-of-plane deformation observable as twisting.^[10,18,20,23]

The work presented here was motivated by a series of recent papers^[24–28] in which Modes and Warner predict that defect-containing LCNs should exhibit mechanically adaptive responses highly distinguishable to any reports to date.^[24] The authors clearly show that sheets composed of glassy LCNs subsumed with a central topological defect and resulting director profile spanning the entirety of the film will result in a complex distribution of strain that concentrates at the defect. The clearest depiction of this is the predictions that subjecting glassy LCN materials patterned with a single +1 topological defect to an appropriate stimulus will cause the sheet to spontaneously morph into a cone with the center of the defect as the apex.^[25] The subsequent papers extended upon these results by introducing the design framework (so-called “grammar and vocabulary”^[28]) surrounding the piece-wise use of topological defects (strengths $|m| \leq 1$) as localized Gaussian curvature building blocks that could be assembled to create pre-programmed, shape-reconfigurable, non-developable surfaces from flat sheets.

One of the salient features of liquid crystalline materials is the ability to readily organize the director profile into complex patterns. Most commonly, director patterning is facilitated by the use of photoalignment surfaces based on azobenzene materials. Domain profile patterning with photoalignment has been recently reported, such as in the fabrication of arrays of axial waveplates.^[36] Recently, Broer and coworkers employed photoalignment to pattern defects into glassy, LCN materials containing a heat transfer dye and demonstrated photothermal formation of cone and anti-cone surface topographies as predicted by Modes and Warner.^[37] Here, we present the systematic examination of topographical transformation resulting from photomechanical response of azo-LCN films with defects ranging from $-5/2$ to $+5/2$, the response of high-strength defects ($|m| = 10$), as well as explore the coordinated response of periodic arrays of topological defects.

Topological defects are of fundamental interest to a variety of areas including mathematics, physics, and materials science (liquid crystals, ferromagnetic, ferroelectrics).^[29,30] In thin, planarly aligned nematic liquid crystals prepared without a preferred orientation (continuously degenerate) they commonly occur in the form of disclinations through which molecular

Dr. M. E. McConney, V. P. Tondiglia,
Dr. K. M. Lee, Dr. T. J. White
Air Force Research Laboratory
Materials and Manufacturing Directorate
3005 Hobson Way, WPAFB, OH, 45434, USA
E-mail: timothy.white.24@us.af.mil



Dr. D. Langley
Air Force Institute of Technology
Department of Electrical and Computer Engineering
2950 Hobson Way, WPAFB, OH 45433, USA
A. Martinez, Prof. I. I. Smalyukh
Department of Physics
Liquid Crystal Materials Research Center
Department of Electrical, Computer and Energy Engineering
and Materials Science Engineering Program
University of Colorado, Boulder
Colorado, 80309, USA
Renewable and Sustainable Energy Institute
National Renewable Energy Laboratory and University of Colorado
Boulder, Colorado, 80309, USA

DOI: 10.1002/adma.201301891

orientation changes discontinuously and span the film thickness running in the direction perpendicular to the film. These defects are ascribed and referred to by defect strength, m , that is defined as the number of rotations of the nematic director orientation, n , around the disclination as one circumnavigates the defect core once.^[31,32] The sign of the defect strength is ascribed based on the direction of director rotation with respect to the direction of circumnavigation about the defect. A positive sign is assigned to director rotations that follow the circumnavigation direction of the point at the center of the defect, whereas a negative sign is assigned for rotations in the opposite direction. The continuous nature of the director rotation about the center of defect and the non-polar symmetry ($\mathbf{n} = -\mathbf{n}$) limits allow defect strengths of integer and half integer values. Defects in liquid crystalline materials can be readily observed under crossed linear polarizers as points at the center of radiating dark brushes in the so-called “Schlieren textures”.^[33] The brushes occur in regions where n is parallel or perpendicular to polarization of the incoming light, where the liquid crystal does not alter the polarization of the incoming light. Therefore the absolute value of the defect strength ($|m|$) can be determined by counting the number of brushes observed under crossed polarizers, N , through the following relation,^[34]

$$|m| = N/4 \quad (1)$$

Allowable, naturally occurring defects in liquid crystalline materials have strengths of $-1/2$, $+1/2$, -1 , and $+1$. Defects with strength $|m| > 1$ are unstable due to the high elastic energy, F , which scales with defect strength as $F \sim m^2$.^[34,35] Due to the fact that we are dealing with lateral dimensions of thin films many orders of magnitude larger than the core size and film thickness, we will neglect discussion of defects that “escape in the third dimension” to form nonsingular configurations with complex structure and assume that the director field is two-dimensional, $n(x, y)$.

Our approach to dictating the topological defects examined here utilize photoalignment materials to generate the desired surface alignment patterns, similar to techniques employed to create axial waveplates^[36,38] and polarization independent LC lenses.^[39] The optical patterning setup passes a blue laser (445 nm) through a half-wave ($\lambda/2$) plate and a cylindrical lens projected onto the LC cell prepared from substrates coated with photoalignment surface material (PAAD-22, purchased from BEAM Engineering for Advanced Measurements). As illustrated in Figure 1, both the $\lambda/2$ plate and the sample cell were mounted on computer-controlled, actuated rotation stages. The $\lambda/2$ plate allows the orientation of the linear polarization of the light to the sample to be rotated. Importantly, a cylindrical lens was used to focus the expanded laser beam into a sharp line ($<50 \mu\text{m}$ width, 1.6 cm length). By rotating the sample with respect to this line, a circular area of the cell was exposed to 445 nm light. Both the orientation of the polarization and the sample were rotated during irradiation. The resulting defect strength was regulated by varying the ratio of polarization rotation rate, R_1 , to sample rotation rate, R_2 , via the following equation, $m = 1 - R_1/R_2$, which is valid for allowable defect strengths (i.e. strength must be an integer or half-integer value). For example, a $+1$ strength topological defect is produced by simply rotating the sample at any angular velocity without rotating

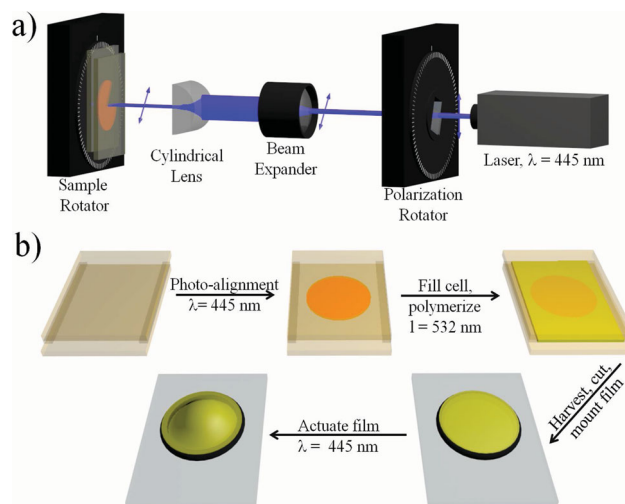


Figure 1. a) A schematic of the optical setup employed to prepare patterned liquid crystal alignment cells. A cylindrical lens focuses the light into a line that the sample was rotated with respect to. By employing a computer-controlled, actuated rotation stage, both the linear polarization and sample were rotated at a determined angular velocity. The defect strength was controlled by the ratio of polarization to sample rotation rates. b) Illustration of the process to prepare, harvest, and characterize defect-patterned azobenzene-functionalized liquid crystal polymer network (azo-LCN) films.

the polarization ($R_1 = 0$). A $+2$ strength defect is produced by rotating the polarization and the sample at the same rate but opposite directions ($R_1/R_2 = -1$). A schematic representation of the sample preparation and harvesting procedure is presented in Figure 1. After patterning the orientation of the surface alignment layer the cells were subsequently filled with the mixture of liquid crystalline monomers and photopolymerized with green light ($l = 532 \text{ nm}$, 35 mW/cm^2 intensity for 30 min) at 75°C (nematic phase). Green light was used to avoid disruption of the photoalignment patterns. After polymerization, the cells were split open and the film was harvested. Polarized optical microscopy (POM) was used to confirm that the polymerized films arrest the defect written into the alignment cell.

Building upon the work of Modes et al.,^[24–28] we report on the photochemically initiated mechanical responses of azo-LCN films subsumed with the director field of a large range of topological defects. Notably, we also extend upon the theoretical predictions as well as the recent experimental examination^[37] by preparing higher order defect strengths not previously considered ($m > |1|$, up to $|10|$). Figure 2 is composed of an illustration of the director field, confirmation of the defect in the circular azo-LCN film by POM (1 cm diameter), a photograph of the observed photomechanical response, as well as an illustration of the observed photomechanical response. Each column is labeled with the defect strength and ratio of rotation rates employed. As is apparent from the polarized optical microscopy images, the generated defects have $N = |m|*4$ brushes. Notably, although each director profile is distinctive—there are observable similarities, for example in the three-fold symmetry of the director orientation of the $+5/2$ defect and the $-1/2$ defect. The origin of the symmetry is more apparent when noting that the R_1/R_2 ratio is equal and opposite between the n -fold pairs.

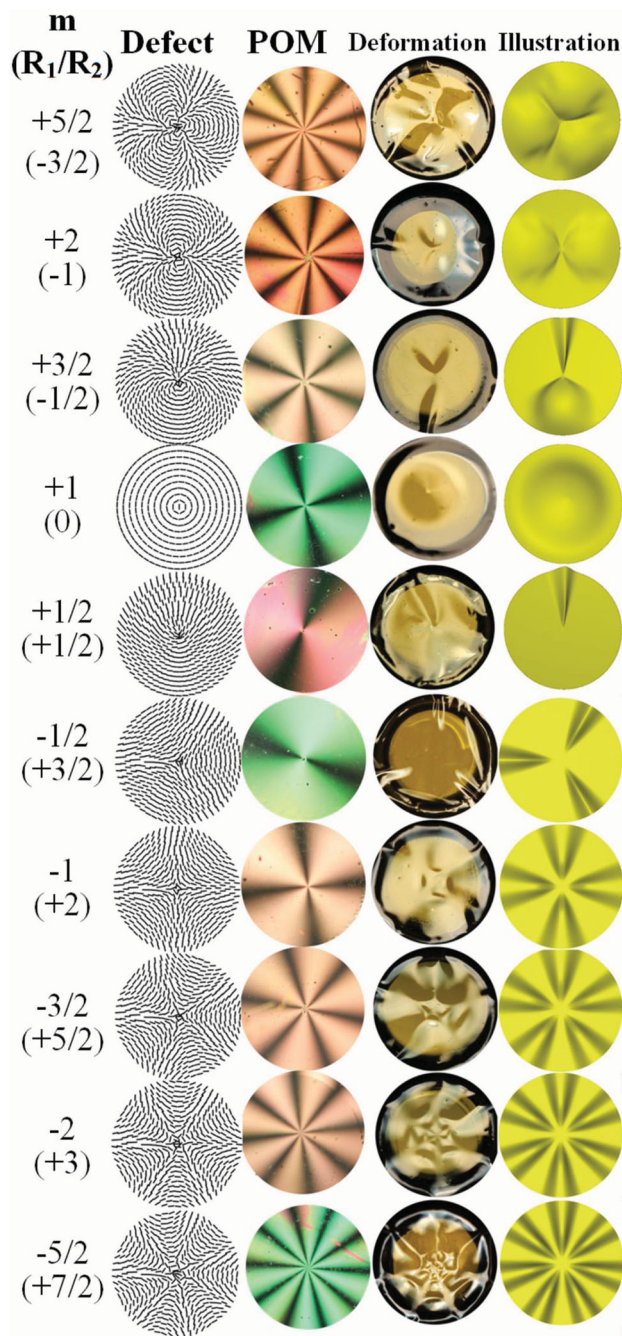


Figure 2. Summary of the director field, polarized optical microscopy image (1 cm diameter), photomechanical response of film (1.2 cm diameter), and illustration of photomechanical response for azo-LCN films subsumed with topological defects ranging from $-5/2$ to $+5/2$ when subjected to unpolarized 445 nm light. The defect strength (m) and ratio of polarization rotation to sample rotation (R_1/R_2) are labeled for each row.

By exposing the photoresponsive, defect-patterned azo-LCN films to unpolarized blue light the materials adopt a complex topography specific to the defect. The underlying photochemical mechanism of transduction of light into mechanical response has been detailed in a number of recent reports^[40] and attributable to local strain generation in the glassy polymer caused by

the reorientation and isomerization of the azobenzene chromophores. Due to the complex alignment of the azobenzene mesogenic units in the azo-LCN, we employed unpolarized light as an isotropic stimulus. The photomechanical response of these films is also illustrated in Figure 2. A description of the photomechanical response of each of these films is included in the Supporting Information. From the images presented in Figure 2 the topographical features formed upon irradiation with 445 nm light are rich and diversified. Close examination of Figure 2 reveals two general trends. First, the deformations of the negatively charged defects follow a clear pattern where the number of equally spaced valleys, V , radiating from the center of the defect is correlated to double the absolute strength of the defect plus two ($V = 2*|m| + 2$ if $m < 0$). Several times the director orientation was tracked throughout the fabrication and deformation process (illustrated in Figure 1). The general trend is the radiating valleys were found to be localized to regions where the director orientation points towards the center of the defect. Second, the deformation of the positively signed defects of strength $m > 2$ where the number of tear shaped dimples, T is related to the defect strength through $T = 2*|m| - 2$ (if $m > 2$). These relationships emphasize that the response of the films is strongly underpinned by the local anisotropy of the director profiles radiating from the topological defect.

Motivated by the complex patterns apparent in the higher-order defects examined in Figure 2, we applied the defect patterning method to form azo-LCN films that retain high-strength defects of $m = \pm 10$. The polarized optical microscopy images presented in Figure 3 confirm that indeed, ± 10 strength defects were retained in the films. As previously mentioned, the elastic energy scales with defect strength as $F \sim m^2$. Therefore, the nematic Frank elastic energy for the $m = +10$ and $m = -10$ defects is roughly two orders of magnitude larger than the other defects examined here. Because of this high energetic cost, these high-strength defects would be unstable in conventional nematic liquid crystal fluids with tangentially degenerate boundary conditions (e.g., in the case of the so-called „Schlieren texture”), however, they are stabilized by the deliberate spatial patterning of the easy axis orientation in the photopatterned alignment cells. Evident in Figure 3, the $m = +10$ defects has eighteen tear shaped nodes, confirming that the above relationship for T holds true despite the considerable increase in elastic energy. The tear shaped nodes are very elongated due to the fact that the director makes a full rotation as one navigates the core every 36° . The -10 strength defect has 22 valleys as shown in Figure 3, also confirming the above relationship for V holds true despite the considerable increase in elastic energy. Notably, the response of the azo-LCN film with a -10 defect has numerous rows of “struts” connecting the expected valleys that radiate from the center of the topological defect. The circumference of the struts spans the entire film and increase in diameter as the distance increases from the center of the defect. Close examination of lower strength defects in the images presented in Figure 2 confirms these struts are also apparent in the -1 , $-3/2$, -2 and $-5/2$ defects (see Supporting Information for further discussion of these features). The scale invariance and self-similar pattern formation apparent in Figures 2 and 3 are also common features of biological systems, especially in response to external stimulus.

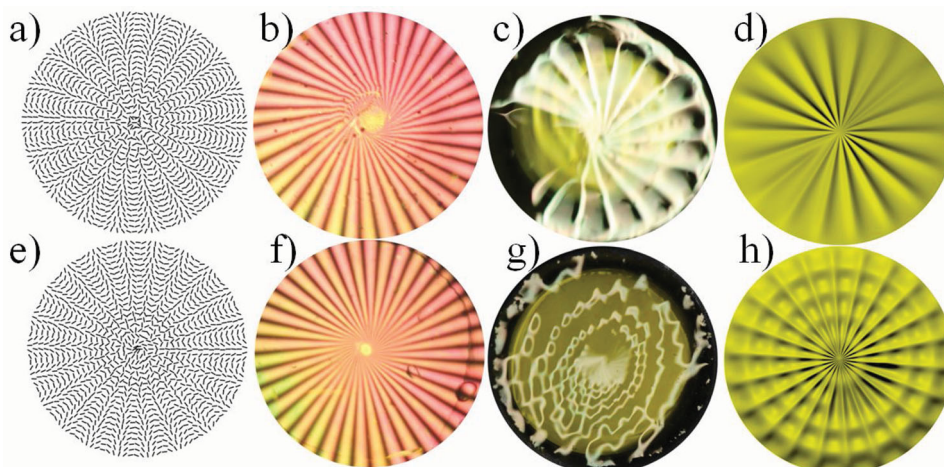


Figure 3. The photomechanical response of azo-LCN films subsumed with high order defects. The director field orientation (a,e), polarized optical microscopy image (1 cm diameter) (b,f), image of the film after photomechanical deflection (1.2 cm diameter) (c,g), and illustration of the photomechanical deflection (d,h) for a +10 defect and a -10 defect, respectively.

An active area of biological research is the role that external mechanical stress plays in mediating scale.

We extend this examination to characterize the response of arrays of „printed” defects. Defect printing was enabled by projecting the 445 nm irradiation through either a +2 or +4 axial waveplate^[36] during photoalignment. The adjacent defects spacing was 3 mm and the diagonal defect spacing was 2.1 mm. The printed defect patterns had a diameter of ~3.1 mm such that the far field of the director profiles overlapped one another. The sample was placed on a motorized stage that allowed for x-y control of the repeated transcribing of the defect pattern onto the photoalignment material. The arrays were printed in a hexagonal pattern and the defects were oriented in the same direction with respect to each other. The resulting complex director field can be interpreted from the photograph imaged of the sample between crossed polarizers presented in **Figure 4**. Upon exposure to unpolarized blue light both the samples demonstrated the expected N-fold topography, with the +2 defects having 2-fold topography and the +4 defect having 6-fold topography. Notably, the hexagonal array of +2 defects results in a square array of 2-fold dimpled geometry. Each defect results in a pair of dimples, thereby effectively cutting the periodic length scale in half along one axis and thus resulting in a square pattern instead of a hexagonal pattern. On the other hand, the hexagonal array of +4 defects, with 6-fold resulting topography, cut the periodic length scale in half along the 3 periodic length scales and thus resulted in a hexagonal pattern. In addition to the patterned positively charged defects, a series of defects having equal net negative charge appear in order to satisfy topological charge/strength conservation, further enriching the photoresponsive topography of these films. The contrast between the resulting topography of these samples serves as an illustrative example of the complexity and richness in transforming the topological patterns in to topographical features.

In conclusion, we show that light can induce rich and diverse topographical transformations of initially flat films composed of photoresponsive, azobenzene-functionalized liquid crystalline

polymer networks (azo-LCN). The topographical response of the defect-containing azo-LCN films was further confirmed experimentally and expanded to examine the response of higher order topological defects that have yet to be considered theoretically or experimentally. Ultimately, the N-fold symmetry of the topography of the photoinduced response of the defect-containing azo-LCN films was inherently coupled to the strength of the defect confirming that the director profile emanating from the topological defect is governing the behavior. The topographical transformation of flat films composed of hexagonal arrays of +2 and +4 topological defects were also presented. This work stands as an experimental demonstration of a ubiquitous approach to forming stimuli-responsive surface topographies and may provide insight into self-assembly processes in nature.

Experimental Section

Optically patternable alignment cells were fabricated by spin coating freshly cleaned pieces of glass with PAAD-22 (purchased from BEAM Co.) at 3000 rpm for 60 seconds. The coated glass substrates were subsequently baked on a hot plate at 100 °C for 10 minutes to evaporate any excess solvent. The two pieces of glass were spaced and glued together by mixing 12 μm cylindrical spacers into an adhesive. Due to slight differences in flatness of the glass and other factors the final cell thickness varied by approximately 1 μm . This small variation in cell thickness was the source of color changes in the cross-polarized images in **Figure 4**, for example.

Optical patterning of the director orientation of the alignment cells was accomplished in a setup employing a blue DPSS laser (445 nm) that was first passed through a $\lambda/2$ plate mounted on an actuated, rotation stage to allow for computer-control of the orientation of the linear polarization of the 445 nm laser to the alignment cell. Subsequent to passing through the $\lambda/2$ plate, the beam was expanded, collimated and focused into a line with a cylindrical lens. The alignment cell was also mounted on an actuated, rotation stage which was rotated at 2°/sec for 180 seconds in all cases. The angular velocity of the rotation of the $\lambda/2$ plate was adjusted to achieve the desired defect strength (governed by $m = 1 - R_1/R_2$). Before the cylindrical lens, the light intensity was 6.5 mW/cm^2 (beam diameter of 1.6 cm). After passing through the cylindrical lens, the focused line had dimensions of approximately 50 μm by 1.6 cm. Because of the Gaussian profile of the laser beam, the

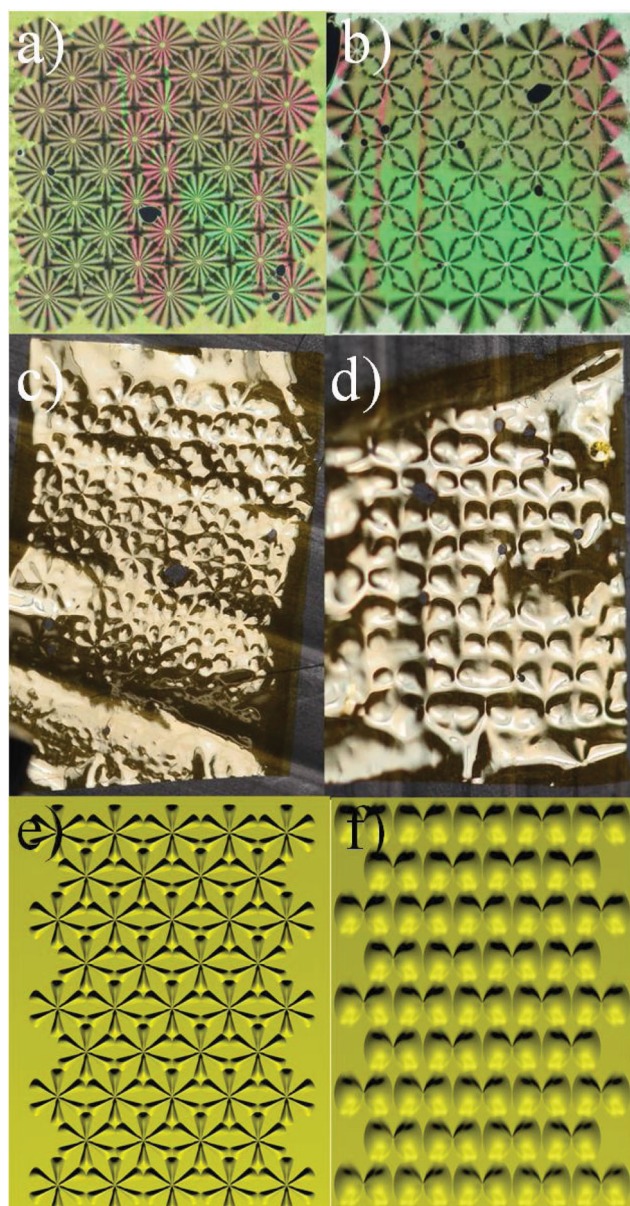


Figure 4. Hexagonal arrays of +2 (left) and +4 (right) topological defects. The top row presents cross-polarized transmission images of defect arrays. The radius of the non-overlapping defects seen at the edge of the array is 1.55 mm. Photographs of the photoinduced deformations of the films are presented in the second row. The samples have a width of 1.6 cm and length of 2 cm. The last row presents schematic representations of the deformation of the arrays.

intensity near the end points of the line was smaller than in the center of the line. Furthermore, in this rotation method the exposure time decreases with increasing distance from the center of the topological defect. Fortunately, the photoalignment material employed here has a large range of exposure conditions in which excellent planar alignment can be achieved. Before and after photoalignment the cell was kept in the dark (hours to days) to avoid room lighting erasing the photoalignment pattern before the cell was filled and polymerized.

The monomer mixture was prepared by mixing 20% A6ZA6 diacrylate azobenzene monomer (BEAM Co.), 78.2% RM 257 diacrylate monomer (Merck), and 1.8 wt% of the visible light photoinitiator Irgacure 784 (Ciba). The mixture of these materials was solid at room temperature.

Special care was taken to mix thoroughly. This mixture was heated into the isotropic phase. The isotropic liquid was placed on the lip of the alignment cell. The monomer mixture filled the photoaligned cells by capillary action in dark room conditions on a hotplate heated to 85 °C. After filling the cell the alignment was checked under cross-polarizers with red lighting. If the alignment of the cell was deemed imperfect the cell was heated to isotropic with a heat gun on the hot plate and allowed to slowly cool to 85 °C. After proper alignment the cell was transferred to a separate hotplate set to 75 °C, allowing the material to cool to the nematic phase. The sample was left for at least 3 minutes to reach this lower temperature. The cell was subsequently exposed to green light ($\lambda = 532$ nm, 35 mW/cm²) for 30 minutes to initiate photopolymerization. Green light was used so as to not impact the photoalignment of the cell.

After photopolymerization, the cells were opened with a razor blade to harvest the films. The films were cut into a circle with the topological defect centered within the circle. To assure that the defect was centered, the film was mounted (still on a piece of glass) at the center of a manual rotation stage. A stationary exacto knife was brought into contact with the film and subsequently the sample was rotated to complete the cut. The samples were cut into circles with a 14 mm diameter. Sample substrates were made by gluing rubber o-rings (inner diameter of 11 mm, outer diameter of 12.5 mm) onto a piece of glass. After the gluing, distilled water was deposited around the outside diameter of the o-ring and then the sample was gently placed onto the o-ring. Care was taken to ensure that the interface between the o-ring and the film was wet. The boundary conditions afforded by this procedure allowed for consistent and repeated demonstrations of the topographical transformations, due to the reduction of friction and allowing the film to be subjected to a uniform and small tensile force. This wet o-ring sample substrate allowed for even capillary forces on the outside of the film and the wet interface allowed for some movement to accommodate photoinduced deflection. The mounted film was exposed to 55 mW/cm² of blue ($\lambda = 445$ nm) unpolarized light from an LED for at least 30 minutes. The newly deformed shape was photographed and analyzed after irradiation. Over several days the amplitude of the deformation nearly disappears, but without cooling the film never fully returns to the flat state. Photogenerated mechanical effects in these materials have been reported to exhibit shape memory behavior.^[19]

Supporting Information

Supporting Information is available from the Wiley Online Library or from the author.

Acknowledgements

This work was completed at the Materials and Manufacturing Directorate of the Air Force Research Laboratory. We thank BEAM Engineering for Advanced Measurements Co. (Nelson Tabiryan) for providing the +2 and +4 axial waveplates. We acknowledge insightful conversations with Carl Modes. This work was supported by the Air Force Office of Scientific Research, Air Force Research Laboratory, and the Air Force Minority Leaders Program. A.M. and I.I.S. acknowledge the support of the COSI program (NSF grant DGE 0801680).

Received: April 27, 2013

Revised: May 29, 2013

Published online: July 21, 2013

- [1] S. J. Woltman, G. D. Jay, G. P. Crawford, *Nat. Mater.* **2007**, 6, 929.
- [2] S. Murata, H. Kurokawa, *IEEE Robot. Autom. Mag.* **2007**, 14, 71.
- [3] A. D. Rey, *Soft Matter* **2010**, 6, 3402.
- [4] Y. Bouligand, *C.R. Chim.* **2008**, 11, 281.
- [5] S. C. Cowin, *J. Non-Newton. Fluid* **2004**, 119, 155.

- [6] D. P. Knight, F. Vollrath, *Philos. T. R. Soc. B* **2002**, 357, 155.
- [7] M. E. McConney, T. J. White, V. P. apg, L. V. Natarajan, D.-k. Yang, T. J. Bunning, *Soft Matter* **2012**, 8, 318.
- [8] K. Urayama, Y. Okuno, T. Kawamura, S. Kohjiya, *Macromolecules* **2002**, 35, 4567.
- [9] K. D. Harris, R. Cuypers, P. Scheibe, C. L. van Oosten, C. W. M. Bastiaansen, J. Lub, D. J. Broer, *J. Mater. Chem.* **2005**, 15, 5043.
- [10] C. L. van Oosten, K. D. Harris, C. W. M. Bastiaansen, D. J. Broer, *Eur. Phys. J. E* **2007**, 23, 329.
- [11] C. L. van Oosten, C. W. M. Bastiaansen, D. J. Broer, *Nat. Mater.* **2009**, 8, 677.
- [12] Y. Yu, M. Nakano, T. Ikeda, *Nature* **2003**, 425, 145.
- [13] M. Yamada, M. Kondo, J.-i. Mamiya, Y. Yu, M. Kinoshita, C. J. Barrett, T. Ikeda, *Angew. Chem. Int. Edit.* **2008**, 47, 4986.
- [14] M. Yamada, M. Kondo, R. Miyasato, Y. Naka, J.-i. Mamiya, M. Kinoshita, A. Shishido, Y. Yu, C. J. Barrett, T. Ikeda, *J. Mater. Chem.* **2009**, 19, 60.
- [15] T. J. White, N. Tabiryan, V. P. Tondiglia, S. Serak, U. Hrozhyk, R. A. Vaia, T. J. Bunning, *Soft Matter* **2008**, 4, 1796.
- [16] T. J. White, S. V. Serak, N. V. Tabiryan, R. A. Vaia, T. J. Bunning, *J. Mater. Chem.* **2009**, 19, 1080.
- [17] S. Serak, N. Tabiryan, T. J. White, R. A. Vaia, T. J. Bunning, *Soft Matter* **2010**, 6, 779.
- [18] K. M. Lee, M. L. Smith, H. Koerner, N. Tabiryan, R. A. Vaia, T. J. Bunning, T. J. White, *Adv. Funct. Mater.* **2011**, 15, 2913.
- [19] K. M. Lee, H. Koerner, R. A. Vaia, T. J. Bunning, T. J. White, *Soft Matter* **2011**, 7, 4318.
- [20] K. M. Lee, T. J. Bunning, T. J. White, *Adv. Mater.* **2012**, 24, 2839.
- [21] T. J. White, *J. Polym. Sci. Poly. Phys.* **2012**, 50, 877.
- [22] K. M. Lee, H. Koerner, D. H. Wang, L.-S. Tan, T. J. White, R. A. Vaia, *Macromolecules* **2012**, 45, 7527.
- [23] Y. Sawa, F. Ye, K. Urayama, T. Takigawa, V. Gimenez-Pinto, R. L. B. Selinger, J. V. Selinger, *P. Natl. Acad. Sci. USA* **2011**, 108, 6364.
- [24] C. D. Modes, M. Warner, *Phys. Rev. E* **2011**, 84, 021711/1.
- [25] C. D. Modes, K. Bhattacharya, M. Warner, *Phys. Rev. E* **2010**, 81, 060701.
- [26] C. D. Modes, M. Warner, C. Sanchez-Somolinos, L. T. de Haan, D. Broer, *Phys. Rev. E.* **2013**, 86, 060701/1.
- [27] C. D. Modes, M. Warner, *Europhys. Lett.* **2012**, 97, 36007/P1.
- [28] C. D. Modes, M. Warner, *Proc. SPIE* **2012**, 8279, 82790Q/1.
- [29] M. Kleman, *Rep. Prog. Phys.* **1989**, 52, 555.
- [30] N. D. Mermin, *Rev. Mod. Phys.* **1979**, 51, 591.
- [31] G. Toulouse, M. Kléman, *J. Phys. Lett.-Paris* **1976**, 37, 149.
- [32] M. Kléman, L. Michel, G. Toulouse, *J. Phys. Lett.-Paris* **1977**, 38, 195.
- [33] P. G. de Gennes, J. Prost, *The Physics of Liquid Crystals*, Clarendon Press, **1995**.
- [34] O. D. Lavrentovich, V. M. Pergamenschchik, *Int. J. Mod. Phys. B* **1995**, 09, 2389.
- [35] F. C. Frank, *Discuss. Faraday Soc.* **1958**, 25, 19.
- [36] S. Nersisyan, N. Tabiryan, D. M. Steeves, B. R. Kimball, *Opt. Express* **2009**, 17, 11926.
- [37] L. T. de Haan, C. Sánchez-Somolinos, C. M. W. Bastiaansen, A. P. H. J. Schenning, D. J. Broer, *Angew. Chem., Int. Edit.* **2012**, 51, 12469.
- [38] S. Nersisyan, N. Tabiryan, D. M. Steeves, B. R. Kimball, *J. Appl. Phys.* **2010**, 108, 033101.
- [39] A. Y. G. Fuh, S.-W. Ko, S.-H. Huang, Y.-Y. Chen, T.-H. Lin, *Opt. Express* **2011**, 19, 2294.
- [40] K. M. Lee, N. V. Tabiryan, T. J. Bunning, T. J. White, *J. Mater. Chem.* **2012**, 22, 691.